Numerical Study of Infinite Wire Radiation Using Finite Differencing Methods

[redacted]†
†Elmore Family School of Electrical and Computer Engineering
Purdue University
West Lafayette, Indiana 47907
E-mail: [redacted]

***Abstract*—Computational finite differencing methods are applied to the case of an infinite current source radiating in multiple different geometries. To apply computational methods, time-stepping formulas that can be iteratively applied are derived from Maxwell's Equations. Perfectly matched layers are used to terminate the simulation region in order to emulate radiation to infinity. The simulation is validated in the cylindrically-symmetric case of a thin, infinite, time-harmonic current source radiating in free space by comparison with the closed-form analytical solution of the geometry. The computational model is then used to study the case of an infinite wire radiating near an infinite perfectly electrically conducting sheet, with one or two slots.**

I. Introduction

The electromagnetic radiation of a thin current source in free space is a commonly studied problem in electromagnetic theory, due to its applicability in the modeling of antennas. Although closed-form solutions for the electric and magnetic fields exist for some source current configurations, such as dipole antennas in free space or near a ground plane [1], a closed-form analytical solution may not exist for arbitrary inhomogeneities in the presence of a source current distribution.

Electromagnetic phenomena are known to be governed to an extremely high degree of accuracy by the set of coupled partial differential equations known as Maxwell's Equations [2]. Because of this, finite differencing methods for numerically solving differential equations are readily applied to the study of electromagnetic phenomena [3]. Here we will apply finite differencing methods to a set of partial differential equations that result from Maxwell's Equations for the situation of interest. The resulting discretized problem is solved by specifying boundary conditions and making use of perfectly matched layers to emulate the geometry existing in infinite free space.

Finite differencing is one of multiple well-known computational approaches for solving electromagnetic problems. This approach approximates differential operators within governing equations to arrive at an ideally iterative solution. It may also result in a linear system that must be solved with other linear algebra techniques. Compared to other computational approaches, such as the finite element method or the method of moments, it is relatively simple mathematically. This allows for faster implementation, making it useful for proof-of-concept studies. Other methods can offer benefits such as being more easily systematically improved, although they can be more difficut and time-consuming to implement. As the name implies, finite-differencing time-domain techniques are also well-suited for time-domain analysis. This can be useful when time-dependent responses are sought, rather than steady-state situations.

II. Formulation and Discretization

To computationally model the desired geometry, we will make use of Maxwell's Equations to generate a set of partial differential equations to be solved, and then discretize the domain to allow for finite differencing methods to be applied to the equations.

A. Mathematical Formulation

To generate equations of interest, we will consider the Maxwell-Ampère equation. This is written in the differential form as

$$\nabla \times \mathbf{H} = \frac{\partial \mathbf{D}}{\partial t} + \mathbf{J} \tag{1}$$

where $\mathbf{H}$ is the magnetic field intensity, $\mathbf{D}$ is the electric displacement field intensity, and $\mathbf{J}$ is the free current density (as opposed to bound current density).

Here we will limit our study to inhomogeneities whose material parameters are linear, time-invariant, and non-dispersive. This allows us to apply linear constitutive relations of the form $\mathbf{D} = \epsilon \mathbf{E}$, where ϵ is the absolute permittivity of the medium, and to write the conduction current using a form of "Ohm's Law," $\mathbf{J}_c = \sigma \mathbf{E}$, where σ is the conductivity of the medium. It is then useful to express the total free current as the sum of the conduction current and an "impressed source current," $\mathbf{J}_i$, which is a free current that we place in the geometry to excite the system. Therefore the total current is expressed as the sum of the impressed source current and any conduction current, such that $\mathbf{J} = \mathbf{J}_c + \mathbf{J}_i$. Under these assumptions, the equation can be rewritten as

$$\nabla \times \mathbf{H} = \epsilon \frac{\partial \mathbf{E}}{\partial t} + \sigma \mathbf{E} + \mathbf{J}_i. \tag{2}$$

We will further specify that we are considering the case of a geometry that is infinite and uniform in one spatial direction. In this case, we can orient our coordinate system such that all quantities of interest are uniform along one axis. We will choose to orient our right-handed x, y, z Cartesian coordinate system such that the z-axis is parallel with the direction of

quantity invariance. We also specify that all source currents ($\mathbf{J}_s$) will be oriented only in the z direction, and be invariant along z. Combining this specification with the implications of equation (2) and the initial condition of zero fields over all space at time $t = 0$, we see that only the z-component of $\mathbf{E}$ and the x- and y-components of $\mathbf{H}$ will be non-zero. Therefore, equation (2) simplifies to the scalar form

$$\frac{\partial H_y}{\partial x} - \frac{\partial H_x}{\partial y} = \epsilon \frac{\partial E_z}{\partial t} + \sigma E_z + J_{i,z}. \tag{3}$$

We will now apply a similar treatment to Faraday's Law, written in differential form as

$$\nabla \times \mathbf{E} = -\frac{\partial \mathbf{B}}{\partial t}. \tag{4}$$

By applying the linear constitutive relation $\mathbf{B} = \mu\mathbf{H}$, where μ is the absolute permeability, and removing the spatial components of $\mathbf{H}$ and $\mathbf{E}$ that are zero, Faraday's Law yields the two scalar relationships

$$\frac{\partial E_z}{\partial y} = -\mu \frac{\partial H_x}{\partial t} \tag{5a}$$

$$\frac{\partial E_z}{\partial x} = \mu \frac{\partial H_y}{\partial t}. \tag{5b}$$

B. Discretization

To develop an iterative method to solve for the quantities of interest, we begin by discretizing the problem. This will be done on the well-known Yee's grid, pioneered in [4]. This discretization scheme makes use of the symmetries present in Maxwell's Equations between electric and magnetic fields by assigning the locations of $\mathbf{E}$ and $\mathbf{H}$ field components on the edges of staggered spatial primal and dual grids respectively. The half-step offset of these grids lends itself naturally to the application of central differencing to the spatial derivatives present in Maxwell's Equations. The fields are also assigned on staggered grids in time, to allow for "leap-frogging" between coupled equations to step forward through time. The discretization geometry will be described here.

Since we are considering the case of infinite uniformity along the z direction, we need only discretize in two spatial dimensions and in time, which allows for simplifications from a full 3D Yee grid. In this case the spatial dimensions to be discretized are x and y. We will divide the region of interest into rectangular cells to form the primal grid, with a length along the x direction of Δx and a length along the y direction of Δy. Therefore, x and y locations on the grid points of the primal grid are of the form $x = i\Delta x$ and $y = j\Delta y$, where i and j are integer indices. We will discretize similarly in time, such that the primal time grid points are at $t = n\Delta t$, where n is also an integer index.

We will assign the spatial locations of E_z to be exactly on the grid points of the 2D primal spatial grid[1], as well as on the primal time grid points. To easily reference the field values at these locations, we will introduce the shorthand

$$E_z(i\Delta x, j\Delta y, n\Delta t) = E_z^n(i, j) \tag{6}$$

to more compactly represent the value of the z-component of the electric field at a spatial grid coordinate (i, j) at time step n.

As for the assignment of the spatial locations of the components of the magnetic field, we first define the dual grid to have grid points that are offset from the primal grid by a half-step in both the x and y directions, such that the spatial locations of the dual grid points are of the form $x = (i + 1/2)\Delta x$, $y = (j + 1/2)\Delta y$, where i and j are once again integer indices[2]. Now, we assign the spatial locations of each vector component of $\mathbf{H}$ to be at the centers of the edges of the dual grid cells that are parallel to that spatial component. The values of $\mathbf{H}$ in time are also assigned to the dual time grid, located a half-step off the primal time grid, at $t = (n + 1/2)\Delta t$.

Using shorthand notation analagous to that in Equation (6), The spatial locations of the components of $\mathbf{H}$ are then assigned at $H_x^{n+1/2}(i, j + \frac{1}{2})$ and $H_y^{n+1/2}(i + \frac{1}{2}, j)$.

C. Time-Stepping Formulation

Since the quantities of interest have been discretized on a regular grid, it is now possible to numerically approximate the derivatives in both time and space in the scalar differential equations (3), (5a), and (5b). We will do so using central differencing, which for the partial derivative in x of some function $f(x, y, t)$ takes on the form [3]

$$\frac{\partial f(x, y, t)}{\partial x} \approx \frac{f(x + \frac{\Delta x}{2}, y, t) - f(x - \frac{\Delta x}{2}, y, t)}{\Delta x}, \tag{7}$$

with derivatives in other quantities taking on analogous forms.

Since we have discretized the problem, we can then use the shorthand notation (as in (6)) to express the central differencing approximation as

$$\frac{\partial f^n(i, j)}{\partial x} \approx \frac{f^n(i + \frac{1}{2}, j) - f^n(i - \frac{1}{2}, j)}{\Delta x}, \tag{8}$$

which can also be applied to derivatives in y and t, which would affect the indices j and n respectively.

To discretize the first scalar differential equation (3) derived from the Maxwell-Ampère equation, we will choose to evaluate the equation at the spatial grid point (i, j), and at the time grid point $n + 1/2$. This is done such that the time derivative will result in the use of values of E_z at time steps n and $n + 1$, as E_z is defined only on integer time steps. For any E_z present in the equation on a half-integer time-step, we will use the arithmetic mean of the available time-steps surrounding the point of interest, such that we substitute $E_z^{n+1/2} \rightarrow (E_z^{n+1} + E_z^n)/2$, preserving second-order accuracy.

[1] On the full 3D grid, values of E_z are assigned at the centers of the edges of the 3D rectangular cells that are parallel to the z direction, putting them a half-step off the primal grid along the z direction. In the 2D case being considered here, we are effectively operating entirely in a plane located one half-step off the full 3D primal grid in the z direction.

[2] In the full 3D grid, the dual grid would be offset from the primal grid by a half-step in all three spatial dimensions.

Applying all of this to (3) results in

$$\begin{aligned}\frac{1}{\Delta x}\Big(H_y^{n+1/2}(i+\tfrac{1}{2},j)-H_y^{n+1/2}(i-\tfrac{1}{2},j)\Big)-\\ \frac{1}{\Delta y}\Big(H_x^{n+1/2}(i,j+\tfrac{1}{2})-H_x^{n+1/2}(i,j-\tfrac{1}{2})\Big)=\\ \frac{\epsilon(i,j)}{\Delta t}\big(E_z^{n+1}(i,j)-E_z^{n}(i,j)\big)+\\ \frac{\sigma(i,j)}{2}\big(E_z^{n+1}(i,j)+E_z^{n}(i,j)\big)+J_{i,z}^{n+1/2}(i,j),\end{aligned} \tag{9}$$

where we have assigned the values of the impressed source current, $J_{i,z}$, to be on the primal grid points spatially, and at half-integer time steps temporally for convenience. This is done because it is present only in the time-stepping equation for E_z, and eliminates the need for any time-averaging on $J_{i,z}$.

Solving the above equation for $E_z^{n+1}(i,j)$ results in the time-stepping formula for E_z

$$\begin{aligned}E_z^{n+1}(i,j)=\frac{1}{\beta(i,j)}\Bigg\{\alpha(i,j)E_z^{n}(i,j)+\\ \frac{1}{\Delta x}\Big(H_y^{n+1/2}(i+\tfrac{1}{2},j)-H_y^{n+1/2}(i-\tfrac{1}{2},j)\Big)-\\ \frac{1}{\Delta y}\Big(H_x^{n+1/2}(i,j+\tfrac{1}{2})-H_x^{n+1/2}(i,j-\tfrac{1}{2})\Big)-\\ J_{i,z}^{n+1/2}(i,j)\Bigg\},\end{aligned} \tag{10}$$

where we have

$$\alpha(i,j)=\left(\frac{\epsilon(i,j)}{\Delta t}-\frac{\sigma(i,j)}{2}\right) \tag{11}$$

and

$$\beta(i,j)=\left(\frac{\epsilon(i,j)}{\Delta t}+\frac{\sigma(i,j)}{2}\right), \tag{12}$$

where $\epsilon(i,j)$ and $\sigma(i,j)$ are used to explicitly indicate the spatial dependence of the permittivity and conductivity.

Applying the discretized central differencing formula (8) to the remaining scalar differential equations (5a) and (5b) derived from Faraday's law, at spatial grid points $(i,j+\frac{1}{2})$ and $(i+\frac{1}{2},j)$ respectively, and at time grid point n, results in similar expressions that can be manipulated to yield time stepping formulas for H_x and H_y of the form

$$\begin{aligned}H_x^{n+1/2}(i,j+\tfrac{1}{2})=H_x^{n-1/2}(i,j+\tfrac{1}{2})\\ -\frac{\Delta t}{\mu(i,j+\frac{1}{2})\Delta y}\big(E_z^{n}(i,j+1)-E_z^{n}(i,j)\big)\end{aligned} \tag{13a}$$

$$\begin{aligned}H_y^{n+1/2}(i+\tfrac{1}{2},j)=H_y^{n-1/2}(i+\tfrac{1}{2},j)\\ +\frac{\Delta t}{\mu(i+\frac{1}{2},j)\Delta x}\big(E_z^{n}(i+1,j)-E_z^{n}(i,j)\big)\end{aligned} \tag{13b}$$

D. Perfectly Matched Layer Region Termination

Since we wish to model the case of a source radiating in free space, we must terminate the discretized region in a way that minimizes artificial reflections, as well as absorbs effectively all of the energy of the wave. To accomplish this, we will use a numerical implementation of a perfectly matched layer (PML), a concept first introduced in [5]. A PML is a simulation region of hypothetical absorbing material that is specifically designed such that there are no reflections on the interface between the region of free-space simulation, regardless of angle of incidence, polarization, and frequency. The material then absorbs enough of the wave's energy to emulate radiation out to infinity. Here we will closely follow the development presented in Section 8.5.3 of [3].

1) Stretched Coordinate Formulation: To begin deriving a way to computationally model some material that can absorb any electromagnetic wave incident upon it, use is made of "stretching" functions along the x, y, and z axes, written as $s_x(x)$, $s_y(y)$, and $s_z(z)$, respectively. By writing a modified form of Maxwell's Equations in this stretched coordinate system, one can derive conditions under which any waves incident upon the boundary between two material regions are guaranteed to be perfectly transmitted. In particular, we find that if (i) the permittivities and permeabilities on either side of the interface are matched, and (ii) the stretching functions parallel to the interface on either side are matched, then perfect transmission is guaranteed to occur. We are then free to assign the third stretching function an imaginary part, introducing loss in the wave. Since the waves are being sufficiently absorbed in the PML region, we may then close off the entire region with a perfectly electrically conducting boundary condition.

2) Numerical Implementation of PML: To actually be able to implement a material region with the properties described above in a finite-differencing scheme, we will first define the stretching functions to have forms analogous to that of a complex permittivity in a lossy medium, such that

$$s_x=1-j\frac{\sigma_x}{\omega\epsilon},\quad s_y=1-j\frac{\sigma_y}{\omega\epsilon},\quad s_z=1-j\frac{\sigma_z}{\omega\epsilon}, \tag{14}$$

which will be convenient in the following development.

Next, we artificially decompose the magnetic field into a number of "split fields", such that $\mathbf{H}_{sx}+\mathbf{H}_{sy}+\mathbf{H}_{sz}=\mathbf{H}$, to conveniently break the full form of Faraday's Law into a set of simpler vector equations more suitable for time-stepping. So, we can decompose the frequency domain differential form of Faraday's Law (noting that in the problem being studied here, only E_z, H_x, and H_y are nonzero) into several equations by expanding the cross product between the new vector nabla operator in our stretched coordinate system, ∇_s, and $\mathbf{E}$, and decomposing the $\mathbf{H}$ field into three split fields corresponding to each term of the expanded cross product. We then rewrite in the time domain to arrive at

$$\frac{\partial}{\partial x}(\hat{\mathbf{x}}\times\hat{\mathbf{z}}E_z)=-\mu\frac{\partial\mathbf{H}_{sx}}{\partial t}-\frac{\sigma_x\mu}{\epsilon}\mathbf{H}_{sx} \tag{15a}$$

$$\frac{\partial}{\partial y}(\hat{\mathbf{y}}\times\hat{\mathbf{z}}E_z)=-\mu\frac{\partial\mathbf{H}_{sy}}{\partial t}-\frac{\sigma_y\mu}{\epsilon}\mathbf{H}_{sy}, \tag{15b}$$

noting from the results of the unit vector cross-products present in (15) that the split components of $\mathbf{H}$ must have the forms $\mathbf{H}_{sx}=\hat{\mathbf{y}}H_{sx}$, $\mathbf{H}_{sy}=\hat{\mathbf{x}}H_{sy}$, and $\mathbf{H}_{sz}=0$.

We can apply the same treatment to the Maxwell-Ampère equation, now splitting the electric field into $\mathbf{E}=\mathbf{E}_{sx}+\mathbf{E}_{sy}+\mathbf{E}_{sz}=\hat{\mathbf{z}}E_z$. Noting that $\mathbf{H}=\hat{\mathbf{x}}H_{sy}+\hat{\mathbf{y}}H_{sx}$, we arrive at

another set of equations

$$\frac{\partial}{\partial x}(\hat{\mathbf{x}} \times \hat{\mathbf{y}} H_{sx}) = \epsilon \frac{\partial \mathbf{E}_{sx}}{\partial t} + \sigma_x \mathbf{E}_{sx} \tag{16a}$$

$$\frac{\partial}{\partial y}(\hat{\mathbf{y}} \times \hat{\mathbf{x}} H_{sy}) = \epsilon \frac{\partial \mathbf{E}_{sy}}{\partial t} + \sigma_y \mathbf{E}_{sy} \tag{16b}$$

where we see from these two equations (16a) and (16b) that $\mathbf{E}_{sx} = \hat{\mathbf{z}} E_{sx,z}$ and $\mathbf{E}_{sy} = \hat{\mathbf{z}} E_{sy,z}$. Combining this with the knowledge that $E_x = E_y = 0$, we know that the third equation resulting from splitting the electric field in the Maxwell-Ampère equation that involves $\hat{\mathbf{z}} \times \mathbf{H}$ and $\mathbf{E}_{sz}$ (not shown above) must be zero on both sides.

Applying the aforementioned simplified forms of the split field vectors and evaluating the cross products in equation set (15) leads to a set of scalar differential equations

$$\frac{\partial E_z}{\partial x} = \mu \frac{\partial H_y}{\partial t} + \frac{\sigma_x \mu}{\epsilon} H_y \tag{17a}$$

$$\frac{\partial E_z}{\partial y} = -\mu \frac{\partial H_x}{\partial t} - \frac{\sigma_y \mu}{\epsilon} H_x. \tag{17b}$$

Applying analogous simplifications to equation set (16) results in a similar set of scalar differential equations

$$\frac{\partial H_y}{\partial x} = \epsilon \frac{\partial E_{sx,z}}{\partial t} + \sigma_x E_{sx,z} \tag{18a}$$

$$\frac{\partial H_x}{\partial y} = -\epsilon \frac{\partial E_{sy,z}}{\partial t} - \sigma_y E_{sy,z}. \tag{18b}$$

Discretizing the fields on spatial and temporal grids in the same way as in section II-B, we may apply the central differencing formula (8) to the simplified scalar relationships between $E_z = E_{sx,z} + E_{sy,z}$, H_x, and H_y. We will apply central differencing in equation (17a) at spatial grid point $(i + \frac{1}{2}, j)$, at time step n, and in (17b) at spatial grid point $(i, j + \frac{1}{2})$, also at time step n. In equation set (18), central differencing will be applied at spatial grid point (i, j), and at time step $n + \frac{1}{2}$. Applying all the conditions described here results in the time-stepping formulas for a PML region for the magnetic field components

$$H_x^{n+1/2}(i, j+\tfrac{1}{2}) = \frac{1}{\beta_y(i, j+\frac{1}{2})}\Big\{\alpha_y(i, j+\tfrac{1}{2}) H_x^{n-1/2}(i, j+\tfrac{1}{2}) - \frac{\epsilon(i, j+\frac{1}{2})}{\mu(i, j+\frac{1}{2})\Delta y}\big(E_z^n(i, j+1) - E_z^n(i, j)\big)\Big\} \tag{19a}$$

$$H_y^{n+1/2}(i+\tfrac{1}{2}, j) = \frac{1}{\beta_x(i+\frac{1}{2}, j)}\Big\{\alpha_x(i+\tfrac{1}{2}, j) H_y^{n-1/2}(i+\tfrac{1}{2}, j) + \frac{\epsilon(i+\frac{1}{2}, j)}{\mu(i+\frac{1}{2}, j)\Delta x}\big(E_z^n(i+1, j) - E_z^n(i, j)\big)\Big\}, \tag{19b}$$

and for the split electric field components

$$E_{sx,z}^{n+1}(i, j) = \frac{1}{\beta_x(i, j)}\Big\{\alpha_x(i, j) E_{sx,z}^n(i, j) + \frac{1}{\Delta x}\big(H_y^{n+1/2}(i+\tfrac{1}{2}, j) - H_y^{n+1/2}(i-\tfrac{1}{2}, j)\big)\Big\} \tag{20a}$$

$$E_{sy,z}^{n+1}(i, j) = \frac{1}{\beta_y(i, j)}\Big\{\alpha_y(i, j) E_{sy,z}^n(i, j) - \frac{1}{\Delta y}\big(H_x^{n+1/2}(i, j+\tfrac{1}{2}) - H_x^{n+1/2}(i, j-\tfrac{1}{2})\big)\Big\}, \tag{20b}$$

where $\alpha_{x,y}(i, j)$ and $\beta_{x,y}(i, j)$ are defined similarly to (11) and (12), where the subscripts now refer to the subscript on σ.

III. Numerical Results

The previously described time-stepping methods were implemented using Python code. All simulations were performed using a frequency of 2.4 GHz. This is an important frequency often used by FCC Part 15 unlicensed wireless communication equipment such as wireless LAN (Wi-Fi) devices. This frequency corresponds to a free-space wavelenth of $\lambda = 12.5\,\text{cm}$.

When discretizing the simulation region, spatial steps were chosen as a certain fraction of a wavelength, such that for all simulations run, spatial step sizes were Δx, $\Delta y < \lambda/20$. Using the spatial steps sizes, a stability condition [3] with a safety factor was used to select a time step interval that will guarantee stability:

$$\Delta t = \frac{0.95}{c\sqrt{\frac{1}{(\Delta x)^2} + \frac{1}{(\Delta y)^2}}} \tag{21}$$

where c is the speed of light in vacuum, equal to exactly 299 792 458 m/s.

A. Validation

To verify the functionality of the implementation, a simple geometry was simulated with a single cell source current in the center of the simulation region. The source current was applied with a tapered sinusoidal temporal profile, of the form

$$J_z(t) = J_{z,0}\left(1 - e^{-\frac{t}{\tau}}\right)\sin(2\pi f t) \tag{22}$$

where τ is chosen to gradually excite the system, and f is our chosen frequency of 2.4 GHz. For all simulations presented, τ was chosen to be one seventh of the time interval simulated. The excitation current amplitude, $J_{z,0}$, was computed based on a total excitation current amplitude of $I = 1\,\text{mA}$ and the area of a single cell, such that $J_{z,0} = I/(\Delta x \Delta y)$. The validation simulation region was bounded with PML regions 15 cells thick. The resulting field distribution is seen in Figure 1.

To further verify proper simulation functionality, a comparison was done with a similar geometry that has a closed-form analytical solution. This is the case of an infinite thin wire radiating into free space. The solution methodology is given in chapter 6, section 5 of [3] for the steady-state time-harmonic case in the frequency domain. The resulting solution for E_z in free space, where the current runs along the z-axis, has the form

$$E_z(\omega) = -\frac{k^2 I}{4\omega\epsilon_0} H_0^{(2)}(k\rho), \tag{23}$$

where ω is the angular frequency of the source curent, k is the wavenumber, which in free space is $k = \omega\sqrt{\mu_0\epsilon_0}$, I is the excitation current amplitude, ρ is the radial distance from

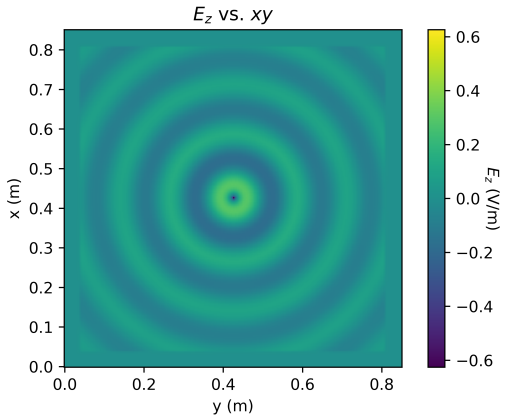

Fig. 1: Result of validation simulation. This is the field distribution at the final time step of a simulation of time interval 2.167×10^{-9} seconds. Here the region was discretized in x and y at an interval of $\lambda/40$. Note that the x direction is plotted along the vertical axis, and the y direction along the horizontal.

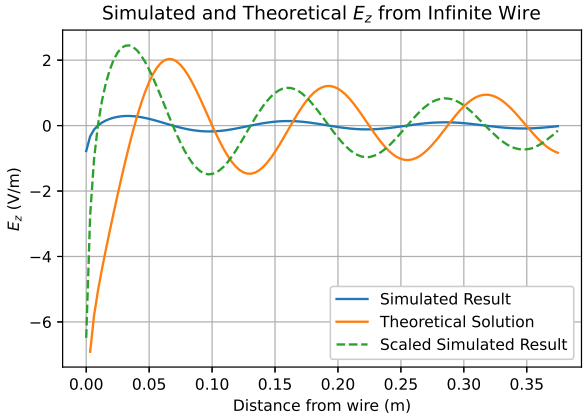

Fig. 2: Plotted curves of $E_z(x)$: simulated (blue), theoretical computed (orange), and scaled simulated (dashed green). The scaled simulated curve is scaled by a factor of 8.33, for better qualitative comparison with the form of the theoretical curve.

the wire, and $H_0^{(2)}$ is the zeroeth-order Hankel function of the second kind.

To represent the solution in the time domain, we take the real part of the product between the phasor and a complex exponential representing the time dependence, expressed as[3]

$$E_z(t) = \mathrm{Re}\left\{E_z(\omega)e^{j\omega t - \frac{\pi}{2}}\right\}. \tag{24}$$

This theoretical solution was computed at the final time step of the system for comparison with the simulated result, as seen in Figure 2.

As is evident in Figure 2, the simulated and theoretical curves are not identical. To a certain extent, this is expected. The theoretical time-harmonic case is strictly valid only for single-frequency excitations. In the time domain, this implies a situation where the source current has been oscillating for all time up to the current moment. The tapered temporal profile and zero-field initial condition in the simulation introduce other frequency components to the system. Some discrepancy between the two is therefore expected, although the difference in magnitude is rather significant. This could be attributed to the finite discretization inherently implying a finite current density over a finite area, as opposed to the infinitely high current density over an infinitesimal area in the theoretical case. Even though both situations are excited with the same total current, a field singularity is allowed in the theoretical case, while in the discretized case it is not.

Qualitatively, the system is otherwise behaving very similarly to the theoretical result. Also plotted in Figure 2 is a scaled version of the simulation result, so as to better compare the spatial profiles of the simulated and theoretical curves. It is seen that the simulated and theoretical curves do indeed have similar spatial profiles.

[3]The $\pi/2$ phase shift in the complex time dependence is included here due to the differing time conventions used in phasor analysis and in this simulation. Standard phasor analysis assumes a time dependence of form $\cos(\omega t)$, whereas the simulated system is excited with a tapered sine function. This is equivalent to a tapered shifted cosine function, as $\cos(\omega t - \pi/2) = \sin(\omega t)$.

B. *Single Slot*

The simulation was run for the case of an infinite wire radiating near an infinitely large perfectly electrically conducting sheet with a single slot. The result is shown in Figure 3. The output behaves as expected, showing diffraction through the slot whose size is smaller than the radiation wavelength.

The diffraction pattern plotted in Figure 4 is also similar to the familiar squared sinc function. It is good to note that this is not expected to coincide perfectly with the usual analytical result, since that approach normally requires the assumption of planar wavefronts impinging on a slot. Here the wavefronts are non-negligibly curved when impinging on the slot, representing a situation that lends itself well to numerical analysis.

C. *Two Slots*

The simulation was run for another case similar to the previous, but now with two slots present. Figure 5 shows the result, once again displaying expected diffraction behavior. One can see that there is slight asymmetry about the center y-axis. This is due to the current source being slightly off-center with respect to the slots. Since there were an even number of cells on the grid along the x-direction, the source could not be placed perfectly between them. This asymmetry is even more prevalent in the diffraction pattern plotted in Figure 6.

Aside from the asymmetry, the double slot diffraction pattern does qualitatively display the expected additional cosine modulation that comes with two-slot interference patterns. This is once again a case that is not expected to coincide perfectly with its analytical solution counterpart, as the wavefronts are curved at the slots.

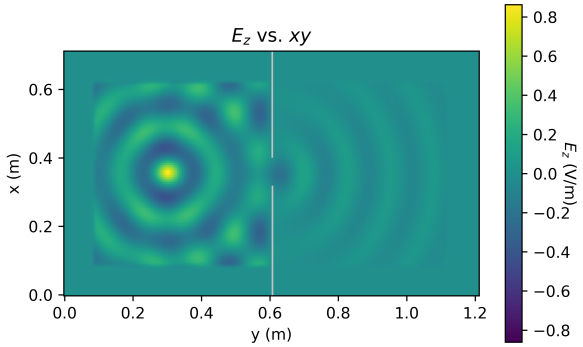

Fig. 3: Result of simulation with a single 7 cm slot in the center of an infinite perfectly electrically conducting sheet a single cell thick. The wire is in the middle along the x direction, and one quarter the length of the entire simulation domain (20-cell-thick PMLs included) along the y direction. The time interval simulated was 4.167×10^{-9} seconds, with spatial grid cell sizes of Δx, $\Delta y = \lambda/25$.

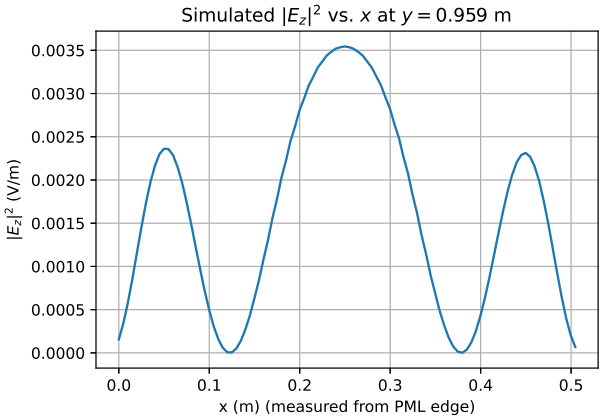

Fig. 4: Plotted squared magnitude of $E_z(x)$ along a cross-section at $y = 0.959$ m after diffraction through a single slot. The squared magnitude is proportional to the intensity, which is how diffraction patterns are normally viewed.

IV. Conclusion

A numerical method was derived from Maxwell's Equations to simulate the time evolution of electromagnetic fields in the presence of inhomogeneities. Measures were also taken to emulate radiation into infinite free space by use of perfectly matched layers. The simulation was shown to be in qualitative agreement with the closed-form solutions of similar geometries.

The current implementation of the numerical method can benefit from further refinement. Specifically, different memory allocation and iteration schemes could be used to reduce the memory and number of calculations needed. Alternative algorithmic approaches with more cases handled explicitly by the programmer could imporove the overall performance.

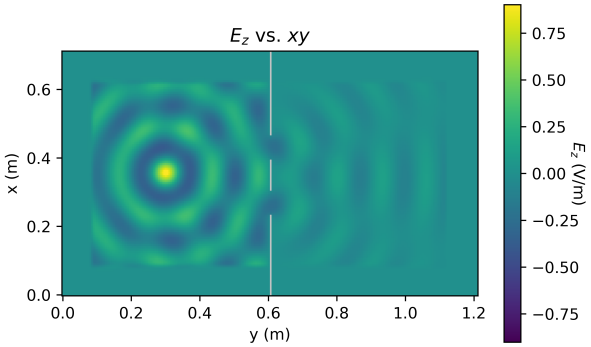

Fig. 5: Result of simulation with two 7 cm slots, spaced such that their centers divide the normal simulation region (not including PMLs) into thirds. The time interval simulated was 4.167×10^{-9} seconds, with spatial grid cell sizes of Δx, $\Delta y = \lambda/25$.

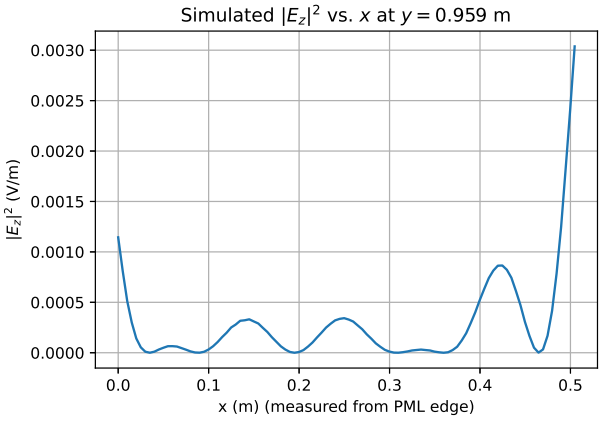

Fig. 6: Plotted squared magnitude of $E_z(x)$ along a cross-section at $y = 0.959$ m after diffraction through two slots.

Additionally, the program's individual functionalities could be better encapsulated. The raw data could be saved by one function or script and passed to another for processing and plotting. This would reduce the number of times the simulation would need to be run to generate the needed plots.

References

[1] C. A. Balanis, *Antenna theory: analysis and design*, 4th ed. John Wiley & Sons, 2015.

[2] J. D. Jackson, *Classical electrodynamics*, 3rd ed. Wiley, 1998.

[3] J.-M. Jin, *Theory and computation of electromagnetic fields*. John Wiley & Sons, 2011.

[4] K. S.-G. Yee, "Numerical solution of initial boundary value problems involving Maxwell's equations in isotropic media," *IEEE Transactions on Antennas and Propagation*, vol. 14, no. 3, pp. 302–307, 1966.

[5] J.-P. Berenger, "A perfectly matched layer for the absorption of electromagnetic waves," *Journal of Computational Physics*, vol. 114, no. 2, pp. 185–200, 1994.